

BRDF EFFECTS IN REMOTELY SENSED HIGH RESOLUTION IMAGES OF URBAN AREAS

Gerhard Meister, André Rothkirch, René Monno, Rafael Wiemker, Johann Bienlein, Hartwig Spitzer
II. Institut für Experimentalphysik
Universität Hamburg
Germany

Mail: G. Meister / KOGS, Vogt-Kölln-Str. 30, 22527 Hamburg, FRG
WWW-Page: <http://kogs-www.informatik.uni-hamburg.de/projects/censis/remotesens.html>
E-mail: meister@informatik.uni-hamburg.de

KEY WORDS: BRDF, Radiometric Measurement, Urban Areas, Surface, Multispectral, Classification

ABSTRACT

Satellite remotely sensed images with a resolution of 1 m are expected to be available in the near future. These images are well suited for the study of inhomogenous areas like cities. This paper presents research projects of our group concerning the bidirectional reflectance properties of man-made surfaces, such as roofs, streets, etc. The BRDF effects (like e.g. specular reflection for forward scattering or Hot Spot for backward scattering) can lead to incorrect classification results. The focus of this paper is the presentation of the measurement of the BRDF of a roof with corrugated tiles.

The distance sensor-target was about 70 m. The sensor consists of two hyperspectral units, measuring from 610 to 1650 nm. The incoming irradiance was determined with a Spectralon panel. Measurements of the shaded roof were used to correct for skylight effects. Particular attention was given to estimating the error, which turned out to be 10 to 12 % on average. The deviation of the measured BRDF values of the roof from Lambertian behavior was 25 % on average, with a maximum of 69 %. We fitted an empiric, analytic function known as 'Walthall model' to the data. We used a version modified to incorporate Helmholtz reciprocity and specular reflection. This function deviates 15 to 20 % on average from the measured roof data, with a maximum of 47 %. The failure of the model to pass a χ^2 test is due to the lack of rotational symmetry of the roof tiles. The specular peak shows a strong increase with wavelength.

Two examples of BRDF effects on asphalt in images acquired with an airborne Daedalus scanner are shown. In the principal plane Hot Spot and specular effects can be seen, in the cross principal plane there is a small increase for large zenith angles.

1 INTRODUCTION

Remote sensing of urban areas demands a very high spatial resolution, because structures like buildings, streets, etc. have diameters of only a few meters. The announcement of satellite data with a pixelsize of about 1 m may make available a large supply of useful data for urban areas. But the small resolution intensifies a problem not so evident using data with a coarse resolution: most roofs are tilted. As the amount of energy received by a roof depends on the cosine of the angle between the surface normal of the roof and the direction of the sunlight, a tilted roof will receive an amount of energy different from its surroundings, and therefore the light reflected from a tilted roof will be different from what is expected assuming flat surfaces. This can lead to considerable errors in classification algorithms based on the reflected light of the surfaces, i. e. most pixel based classification procedures. Yet another effect enhances the problem: most real surfaces do not meet the Lambertian assumption, i. e. the intensity of the reflected radiance depends on the angles of reflection and is not a simple function of the cosine of the incident irradiance.

The directional dependencies of light reflected from a surface are described by the Bidirectional Reflectance Distribution Function (abbreviation: BRDF, symbol: f_r , unit: [1/sr]) as defined by [Nicodemus, 1970]. The BRDF is the ratio of the radiance reflected from a target divided by the incoming irradiance. The BRDF of a surface is a function of the angles of incidence and reflection and of the wavelength.

In this paper we present a study concentrating on measuring and describing the BRDF of a real roof, measured with a hyperspectral sensor at a distance of about 70 m. Preliminary

results of BRDF effects as seen on imagery acquired by airborne scanners are presented too, as well as an outlook for our future activities in this area.

2 BRDF MEASUREMENT OF SEVERAL SAMPLES

In a previous study [Meister, 1996] the BRDF of 6 targets typical for urban areas were measured. Small samples, that fulfilled the requirements of being flat and having rotational symmetry, were put on a goniometer and the reflected radiance was measured. The incoming irradiance could be determined by a Spectralon reference panel. To eliminate skylight effects, the samples were cast in shade and the remaining reflected radiance was subtracted from the previous measurement in sunlight. The following empirical function was fitted to the measured BRDF values:

$$f_r = a_0 + a_1 \cdot (\theta_i^2 + \theta_r^2) + a_2 \cdot (\theta_i^2 \cdot \theta_r^2) + a_3 \cdot (\theta_i \cdot \theta_r) \cdot \cos \varphi + a_4 \cdot e^{a_5 \cdot (\theta_i \cdot \theta_r)^2} \cdot e^{-a_6 \cdot \psi^2} \quad (1)$$

θ_i and θ_r are the zenith angles of the incident and reflected radiation ($\theta_r = 0^\circ$ means viewing from nadir). $\varphi = |\Phi_i - \Phi_r|$ is the relative azimuth. ψ is the angle between the reflected light (direction $\theta = \theta_r, \varphi = |\Phi_i - \Phi_r|$) and the specular angle ($\theta = \theta_i, \varphi = 180^\circ$) (direction of the incident radiation: $\theta = \theta_i, \varphi = 0^\circ$). a_0 to a_6 are coefficients depending on wavelength.

This model was originally proposed by [Walthall, 1985] and modified by [Liang, 1994] to account for Helmholtz's theorem

of reciprocity. We included a Gaussian peak in the specular direction [Meister, 1996]. No measurements could be made close to the Hot Spot region. A Hot Spot peak was therefore not included into the model.

The measured values passed a χ^2 test for this function. As the average error of the measured values was less than 10 %, this shows the good agreement between model and experiment.

Neglecting the specular peak, the BRDF effects of the samples were usually smaller than 15 %. The intensity of the specular peak increased strongly for high zenith angles.

3 BRDF MEASUREMENT OF A REAL ROOF

In a diploma thesis [Rothkirch, 1997], the BRDF of the roof shown in figure 1 was measured. This roof was chosen because the different parts of the roof are orientated in different directions, the total number of different orientations being 4. The sensor was placed on a roof terrace of a nearby skyscraper, the distance between the roof and the sensor was about 70 m. For this distance, the field of view of our sensor has a size of about $0.33\text{m} \times 0.33\text{m}$. The picture of figure 1 was taken from the position of the sensor, the numbers on the roof indicate the different chosen points (total of 9). Although the orientation of the roof at e.g. points 4 and 5 are the same, the angles of reflection differ, 10.8° for the zenith angle θ_r in this case.

We assumed that each of the points has the same BRDF, so that we could measure the BRDF of the roof at 9 different angles of reflection. This assumption is acceptable, since the roof was made of the same kind of tiles at each point.

The roof itself consists of almost sinus-shaped tiles, with a 'wavelength' of 177 mm and an amplitude of 25.5 mm. The color of the tiles is wine-red. The shape of the tiles prevents the roof from having rotational symmetry.

Figures 2 and 3 show the different angles of measurement in the frame of reference of the respective roof parts. Figure 2 shows the angles of reflection (θ_r and Φ_r), 9 points altogether.

Figure 3 shows the angles of incidence (θ_i and Φ_i). 4 different courses of the sun can be seen in this picture, because there are 4 different inclinations of the roof parts, see figure 1 (e.g. point 4 and point 5 have the same inclination). The total number of measurements with different combination of angles equals the number of stars in figure 3, 139.

We used a spectrometer called OVID (Optical Visible and near Infrared Detector) from the Institute of Meteorology of the University of Hamburg and the Max-Planck-Institute for Meteorology, Hamburg, who we want to thank for their cooperation. It consists of two separate units, one for the spectral range 600 nm to 1000 nm with a maximum of 1024 channels, the second for the spectral range 1000 nm to 1650 nm with 256 channels [Bartsch, 1994]. We mounted a telescope on top of the optical units to orientate the sensors to the respective points on the roof. Repeated orientations to the same point at short time intervals showed a repeatability accuracy better than 2 %.

To determine the incoming irradiance for each part of the roof, we used a Spectralon reference panel and corrected for



Figure 1: Investigated roof with measured points

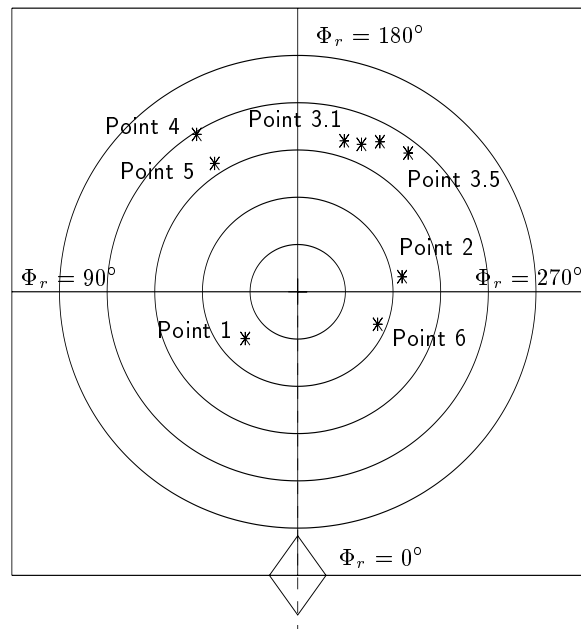


Figure 2: Polar plot of the angles of reflectance. Circles correspond to constant zenith angle, the innermost circle means $\theta_r = 15^\circ$, the outermost 75° . At the rhombus the azimuth Φ_r is zero. The corrugated tiles are orientated so that the crest is vertically.

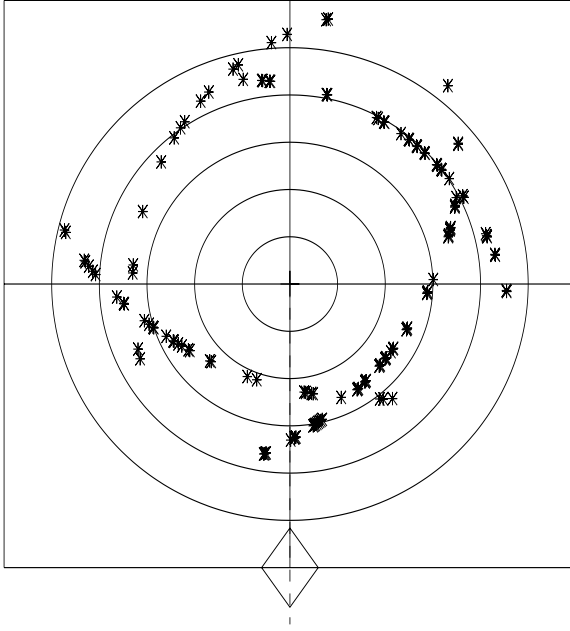


Figure 3: Polar plot of the angles of incidence. Circles correspond to constant zenith angle, the innermost circle means $\theta_i = 15^\circ$, the outermost 75° . At the rhombus the azimuth Φ_i is zero. The corrugated tiles are orientated so that the crest is vertically.

the different inclinations of the roof:

$$E_i^{\text{roof}} = \frac{(L_r^{\text{panel-sunlight}} - L_r^{\text{panel-shaded}})}{f_r^{\text{panel}}} \times \cos \theta^{\text{roof}} \quad (2)$$

The BRDF of the Spectralon panel f_r^{panel} was measured before in the laboratory [Meister, 1996].

The definition of the BRDF involves the radiance from a single direction. In situ measurements always involve skylight, in our case about 20 % of the incoming irradiance were due to skylight. In previous studies, we cast the object under investigation in shade and subtracted the reflected radiance under shade from the reflected radiance in sunlight in order to obtain that part of the reflected radiance coming directly from the sun. We had no means of casting shadow onto the roof at our will, so we had to interpolate the shade measurement from a measurement in the morning, when the nearby skyscraper put the roof into shadow. We performed 5 different kinds of measurements:

1. Unique measurement of the points while being cast in shade in the morning from the nearby skyscraper ($L_r^{\text{roof-shaded}}$)
2. Unique measurement of the reference panel cast in shade shortly afterwards ($L_r^{\text{panel-and-roof-shaded}}$)
3. Measurement of the chosen points on the roof in sunlight ($L_r^{\text{roof-sunlight}}$)
4. Measurement of the Spectralon panel in sunlight afterwards ($L_r^{\text{panel-sunlight}}$)

5. Measurement of the Spectralon cast in shade shortly afterwards ($L_r^{\text{panel-shaded}}$)

(The Spectralon panel was lying close to the sensor on the roof terrace.) Measurement 1 was multiplied by the ratio of measurement 5 over measurement 2 to obtain an interpolated shade measurement of the roof at the time of measurement 3. This interpolated shadow measurement was subtracted from measurement 3 to yield the reflected radiance without skylight effects. This spectrum was divided by the incoming irradiance E_i^{roof} calculated above (equation 2) to yield the BRDF value f_r^{roof} :

$$L_r^{\text{roof-shaded-interpolated}} = L_r^{\text{roof-shaded}} \times \frac{L_r^{\text{panel-shaded}}}{L_r^{\text{panel-and-roof-shaded}}} \quad (3)$$

$$f_r^{\text{roof}} = \frac{L_r^{\text{roof-sunlight}} - L_r^{\text{roof-shaded-interpolated}}}{E_i^{\text{roof}}} \quad (4)$$

We estimated the relative error of $L_r^{\text{roof-shaded-interpolated}}$ to about 18 %. The portion of skylight relative to direct sunlight varied between 10 and 25 % during the day of measurement, so that the overall error due to skylight remained lower than 5 %.

The time difference between the measurement of the roof and the Spectralon reference panel was so big, that we decided to correct the incoming irradiance E_i^{roof} by means of a pyranometer. During all the measurements the global illumination was recorded with a pyranometer. The exact algorithm can be found in [Rothkirch, 1997], it is an interpolation between two succeeding measurements of the Spectralon panel corrected with the pyranometer. The overall error of the incoming irradiance E_i was estimated to be 9.2 %. The total errors of the BRDF values are about 10 to 12 %.

4 DISCUSSION OF THE ROOF MEASUREMENTS

4.1 Specular peak

The BRDF of the investigated roof shows a very non-Lambertian behaviour, the average deviation from a Lambertian BRDF is about 25 %. The measured BRDF values of two points on the roof are shown in figures 4, 5, 6 and 7. The 2 dimensional plots show the measured BRDF values as a function of the relative azimuth between the directions of incidence and reflection, calculated in the frame of reference of the respective roof part. The bars indicate the errors of the BRDF value. Notice that the 2 dimensional plot does not show the influence of the incident zenith angle (the reflected zenith angle is constant for each point). The effect can be seen by comparing figures 5 and 7. Although in each figure at a relative azimuth angle close to 180° measurements were done, only figure 7 shows an increase towards the specular direction. As can be seen from figures 4 and 6, the reason is the difference in zenith angles: the incident zenith angle θ_i closest to the specular direction and the view zenith angle θ_r are both close to 50° in figure 6, but very different in figure 4: $\theta_r \approx 30^\circ$ and $\theta_i \approx 50^\circ$. So only in figures 6 and 7 the effect of a specular peak can be seen.

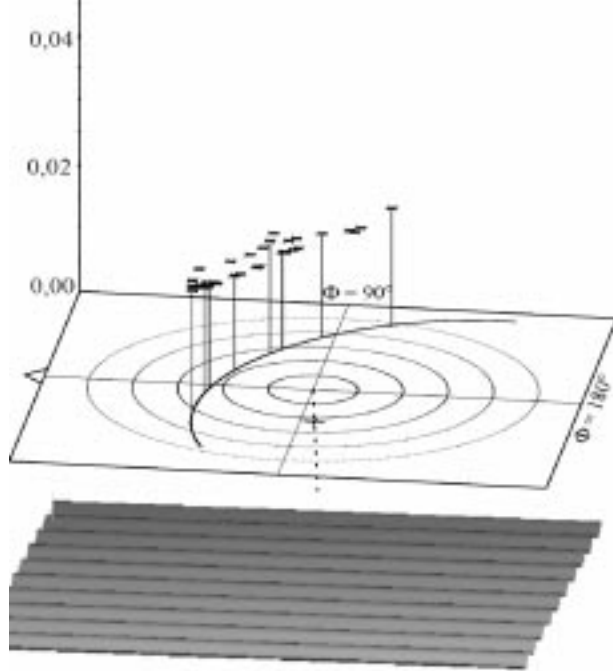


Figure 4: Measured BRDF values at wavelength $\lambda = 1540$ nm of point 2 as a function of incident azimuth and incident zenith angle. The circles are lines of constant θ_i , first circle corresponds to 15° , second circle to 30° , outermost circle to 75° . The arrow on the left shows $\Phi = 0^\circ$, parallel to the crest of the sinus of the roof tiles, the orientation of the tiles is shown below. $\Phi = 90^\circ$ and $\Phi = 180^\circ$ are marked in the plot. The cross shows the angle of the sensor, $\theta_r = 33^\circ$ and $\Phi_r = 262^\circ$ in this case. The z-axis shows BRDF values in [1/sr].

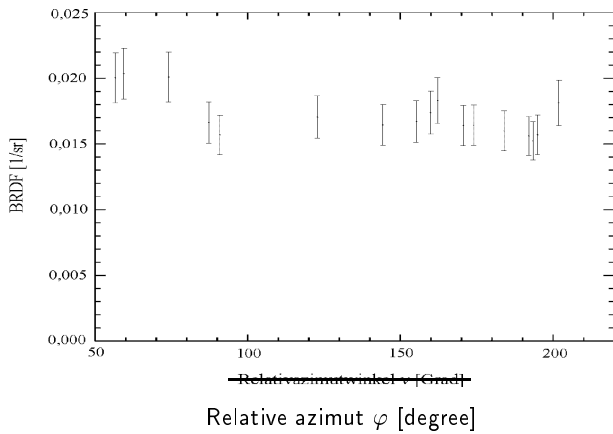


Figure 5: Measured BRDF values at wavelength $\lambda = 1540$ nm of point 2 over relative azimuth $\varphi = |\Phi_i - \Phi_r|$.

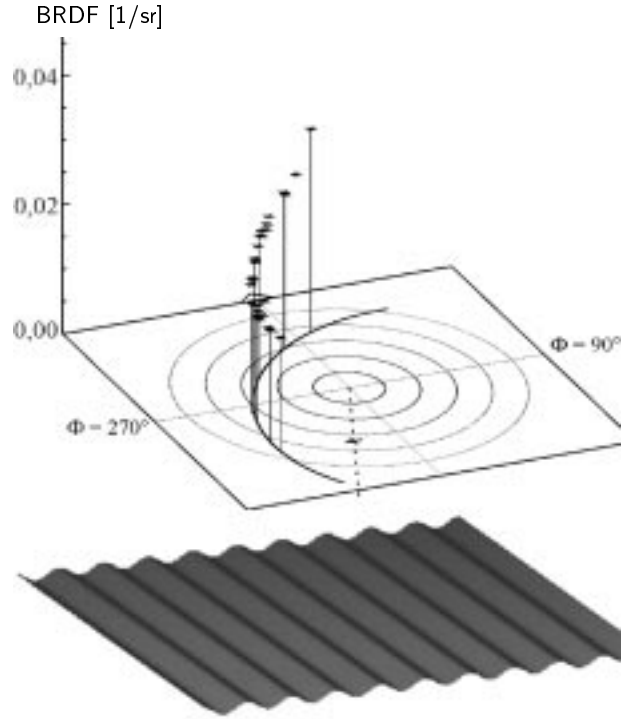


Figure 6: Measured BRDF values at wavelength $\lambda = 1540$ nm of point 3.2 as a function of azimuth and zenith angle, $\theta_r = 51^\circ$ and $\Phi_r = 203^\circ$ in this case. (For an explanation of the axes see figure 4).

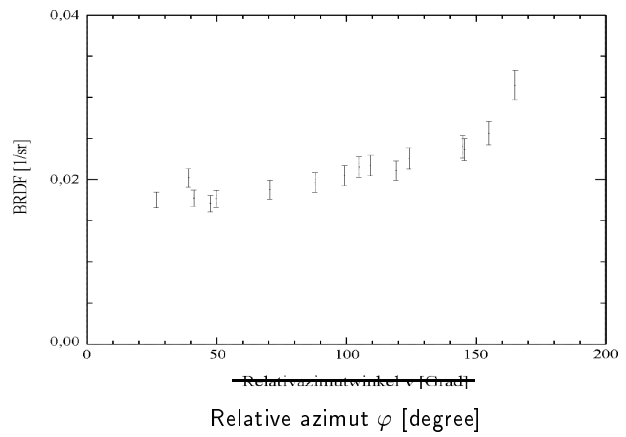


Figure 7: Measured BRDF values at wavelength $\lambda = 1540$ nm of point 3.2 over relative azimuth $\varphi = |\Phi_i - \Phi_r|$.

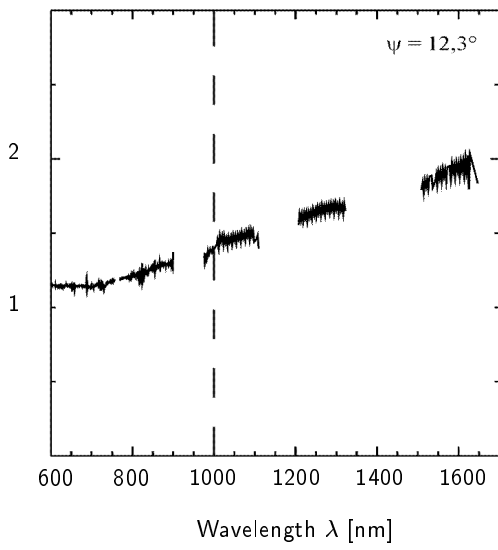


Figure 8: Ratio of a specular ($\theta_i = 54.3^\circ, \Phi_i = 8.2^\circ, \theta_r = 50.9^\circ, \Phi_r = 203.2^\circ, \Psi = 12.3^\circ$) and a nonspecular ($\theta_i = 53.5^\circ, \Phi_i = 250.7^\circ, \theta_r = 50.9^\circ, \Phi_r = 203.2^\circ, \Psi = 92.6^\circ$) measurement versus wavelength. ψ is the relative angle between ideal specular direction and the direction of reflection, see explanations for equation 1.

Figure 8 shows the wavelength dependence of the specular peak. A measurement at a combination of angles close to ideal specular direction ($\psi = 12.3^\circ$) was divided by a measurement of diffuse scattering ($\Psi = 92.6^\circ$). The ratio is almost one at 600 nm and constant, but starts increasing at 700 nm. This increase agrees with Rayleigh's criterion on smooth surfaces:

$$\sigma < \frac{\lambda}{8 \cdot \cos \theta_i} \quad (5)$$

where σ characterizes the roughness of the surface. According to this equation, the 'smoothness' (and therefore the intensity of a specular peak) increase with wavelength, as can be seen in figure 8.

4.2 Fits of models to the data

Several models were fit to the data. No fit passed the χ^2 test. The best fit was produced by the model Meister described in equation 1. The coefficients of the model are shown in table 1. Figure 9 shows the results for a wavelength of 1050 nm. For some of the chosen points on the roof there are obvious disagreements between model and measurements: most of the measurements of point 3.5 (t35 in the figure) are too high, for point 5 (t5 in the figure) they are too low. We believe that the main reason for the failure of the model to describe the measurements is the lack of rotational symmetry of the roof. Dividing the points into 2 groups (according to the orientation of the crest of the tiles, horizontal or vertical in figure 1) and fitting the coefficients of model Meister to each group separately made the model pass the χ^2 test for some wavelengths, but not for all. In some cases, the coefficient a_0 was zero. This is highly unlikely and probably due to either problems with the fitting routine or a bad angular distribution of measurements, so these results are not presented here. Still this indicates that a model not restricted to rotational symmetry will do better than the model Meister.

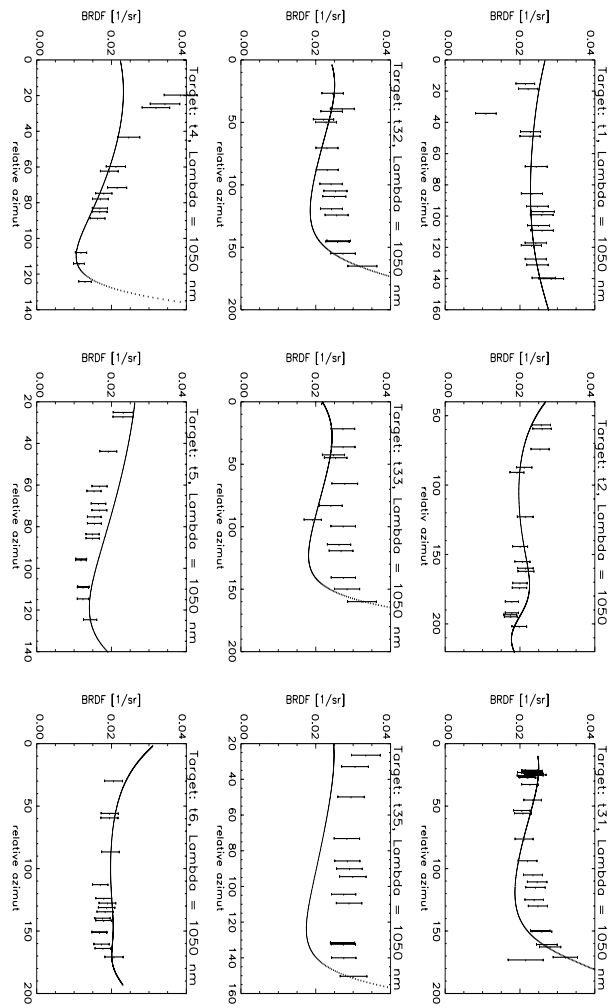


Figure 9: Measured data (with error bars) and fitted model (solid line) for all points at a wavelength of 1050 nm as a function of relative azimuth angle.

The tiles are sinus-shaped and therefore do not have rotational symmetry (e.g. the tiles shown in figure 4 are orientated differently towards the observer than the tiles in figure 6). We are planning to test empirical models that do not only depend on the relative azimuth $\varphi = |\Phi_i - \Phi_r|$ but on Φ_i and Φ_r explicitly, thus modeling surfaces without rotational symmetry.

We developed a BRDF model especially for sinus-shaped, lambertian surfaces, considering masking and shadowing, but not multiple scattering. For the most part, the modeled BRDF is constant, so the deviations of points 3.5 and 5 cannot be explained simply by the sinus shape of the tiles. A strong effect can only be seen for point 4. The BRDF predicted by the Sinus-Lambert model for the angle of reflection of point 4 is shown in figure 12. Notice the increase of the modeled BRDF towards small relative azimuth angles of about a factor 2 between the angles of the lowest and the highest measured value for point 4. Still the measured BRDF values show a much larger increase, about a factor 3 (see figure 9, 'target: t4').

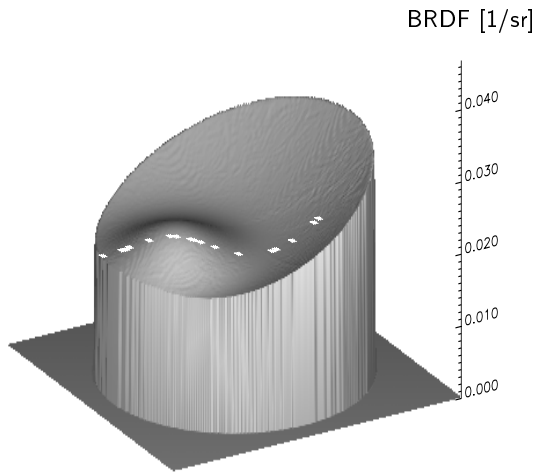


Figure 10: Model Meister fitted to the measurements, displayed for the angles of reflection of point 2 (cf. figure 4). This plot was turned around the z-axis to improve the visual impression. The small 'hill' on the left is the specular peak. The stars show the angles of measurement (but NOT the measured values, they are shown in figure 9).

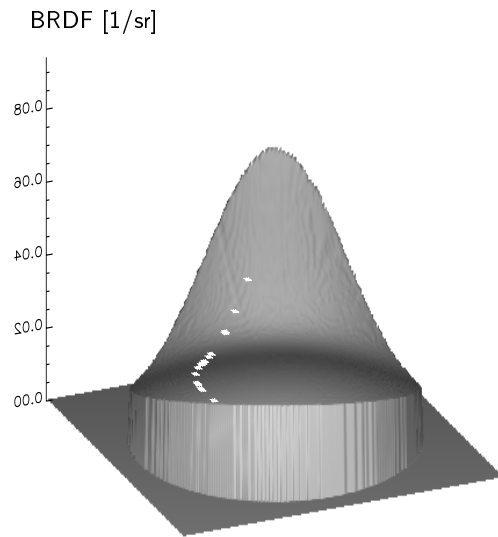


Figure 11: Model Meister fitted to the measurements, displayed for the angles of reflection of point 3.2 (cf. figure 6). This plot was NOT turned around the z-axis, so that the observer is looking from backscatter direction onto the plot, like in figure 6. The very strong increase towards the back of the plot is the specular peak. The stars show the angles of measurement (but NOT the measured values).

Fitting the model of equation 1 to the data is an improvement to assuming a lambertian BRDF, the average deviation of the model from the data is 15 to 20 %, depending on wavelength (compare this to the deviation of the data from a lambertian BRDF, 25 %). The maximum deviation is reduced from 65 % for the Lambertian BRDF to 45 % for our model.

a_0	0.0149	sr^{-1}
a_1	0.0089	$\text{sr}^{-1} \cdot \text{rad}^{-2}$
a_2	-0.018	$\text{sr}^{-1} \cdot \text{rad}^{-4}$
a_3	0.011	$\text{sr}^{-1} \cdot \text{rad}^{-2}$
a_4	0.0058	sr^{-1}
a_5	2.16	rad^{-4}
a_6	3.16	rad^{-2}

Table 1: Coefficients of the fit of model Meister (angles are in radians) at a wavelength of 1050 nm

Figures 10 and 11 show the model Meister fitted to the measurements. The white stars indicate the angles of measurement, their height does **not** show the measured value, but the fitted model. They are shown to make it possible for the observer to judge which features of the fitted model are due to measurement and which ones are interpolated or extrapolated from other measurements (in this case our model must be treated cautious, because it is only an empirical model). E.g. the strong increase with high zenith angles of the specular peak in figure 11 could not be verified by measurements.

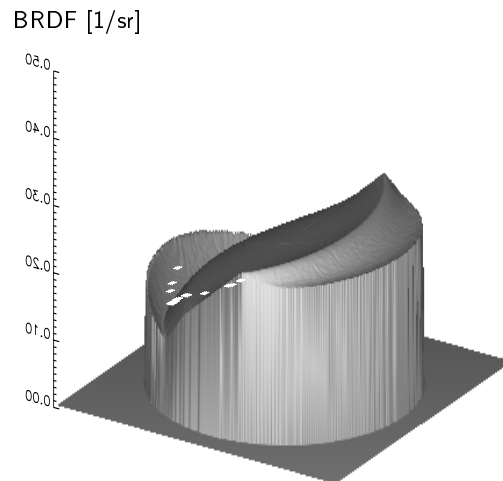


Figure 12: Sinus-Lambert-BRDF-model for the angle of reflection of point 4 ($\theta_r = 59.2^\circ, \Phi_r = 147.5^\circ$). The axes of this plot are the same as in figure 4, the maximum zenith angle is 75° . The observer is looking onto the plot from backscatter direction, as in figures 4 and 6. The stars show the angles of measurement (but NOT the measured values).

4.3 Variance of the different points for changing sun angles

Figure 13 shows the variance of the data after different steps of processing. In all the plots, the variance of the measured reflected radiances of each point is shown for a wavelength of 1008 nm, no corrections for skylight were applied here. The columns on the right ('All points') show the variance with respect to the average over all points.

In the last row, no correction to the sun position was made at all. The second row (darkest columns) shows the measured radiances after dividing by the cosine of the sun zenith angle in world coordinates ($\theta_i = 90^\circ$ meaning sunset or sunrise). The variance of every point has been reduced by about 10 % on average. In the first row (brightest columns), the measurements have been divided by the cosine of the sun zenith angle in the frame of reference of the respective roof part. In case the roof was a perfect Lambertian surface, this would result in the disappearance of the variance (neglecting measurement errors). Some of the points show a reduction of the variance by another 10 %, but for some points the variance increases. The most striking increase has point 4, for this point the variance gets even larger than in the last row, where no corrections at all had been made. The large variance of this point can be explained by the strong non-Lambertian behaviour of the BRDF of a sinus-shaped surface, that was predicted by our Sinus-Lambert model mentioned above.

This diagram shows the difficulties encountered classifying urban areas: even after dividing by the cosine of the sun zenith angle in world coordinates (which usually can be done easily), the variance of the measurements is still about 25 % for each part of the roof and about 40 % for 'All points'. The correction for the inclination of the roof (which usually cannot be done easily since the inclination of the roof is usually not known) results in a variance of about 15 % or less for most points on the roof, but there are exceptions like point 4. The variance of 'All points' reduces to 25 %.

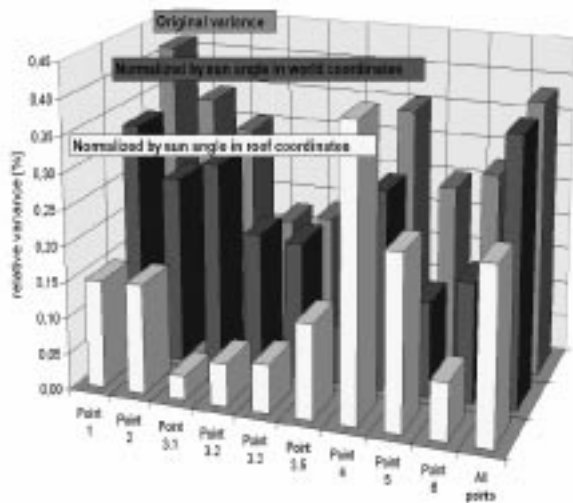


Figure 13: Relative variance of the measured radiances in % for a wavelength of 1008 nm (without corrections for skylight).

5 BRDF EFFECTS IN DATA FROM AN AIRBORNE SCANNER

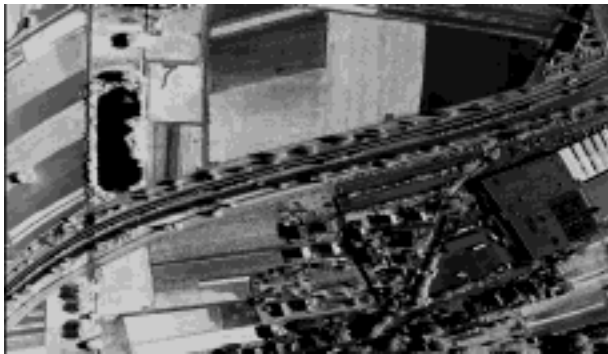
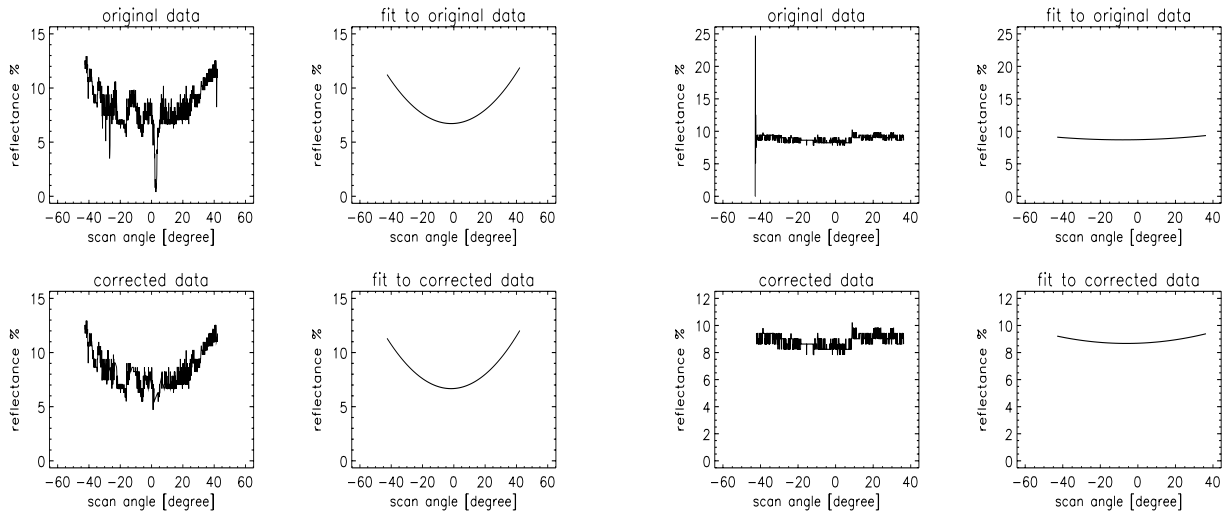
We started a study to investigate the BRDF effects occurring in image data. The data consists of multispectral images from several years acquired with the airborne scanner Daedalus AADS 1268 over Nuremberg, FRG. The flight height was 300 m, resulting in a nadir pixelsize of $0.7 \text{ m} \times 0.7 \text{ m}$, the maximum scan angle of $\pm 43^\circ$ is divided into 716 pixels. The reflected radiances were converted to reflectances using the software package SENSAT-5 based on the radiative transfer simulation program LOWTRAN-7 [Richter, 1994], [Hepp-94] and corrected by ground reference measurements [Kollewe-96]. Daedalus AADS 1268 measures the reflected radiances in 10 different channels, covering wavelengths from 420 to 2350 nm.

Our approach was to look for homogenous, man made surfaces in the images that were so large that they were scanned under different angles. In our data, only streets (or runways on an airport) were large enough to be scanned with different angles. We cut out a line from these areas and plotted the radiances against the scan angle and fitted the original walthall model

$$f_r = a_0(\theta_i) + a_1(\theta_i) \cdot \theta_r^2 + a_2(\theta_i) \cdot \theta_r \cdot \cos \varphi \quad (6)$$

to the data, see figures 14 and 15. In this model, the coefficients a_i vary for different θ_i . We did not fit the model Meister of equation 1 because in each image the sun zenith angle θ_i is constant and the angles corresponding to the pixels on the chosen lines were not close to the specular peak.

It was almost impossible to find homogenous areas in our images. Usually there are some pixels on that line who are obviously made of a material different from their surroundings (e.g. the downward peak in the center of the plot 'original data' in figure 14). We skipped these pixels. The decision if a pixel should be skipped or not was based on the deviation of the reflectance of that pixel to the fitted model, if the difference was bigger than one standard deviation the pixel was skipped, as well as the 2 surrounding pixels. Only the 6 channels corresponding to wavelengths between 520 nm and 1050 nm were chosen, because the noise in the other channels was too big.



1994/nuer04.tif-adj.Autobahn

Figure 14: From this image, a line on the highway (crossing the picture from bottom left to top right) was cut out, the line is indicated by the solid white line. The sun zenith angle is 59.2° . The flight direction is from bottom to top, so the scan direction is from left to right. A vertical line in the center of the picture corresponds to nadir ($\theta_r = 0^\circ$). Scan angles to the left are indicated by negative zenith angles in the plots above and correspond to backscatter direction ($\varphi = 4.5^\circ$), scan angles to the right have positive zenith angles and correspond to forward scattering ($\varphi = 175.5^\circ$). The data are plotted for a wavelength band 630 to 690 nm.

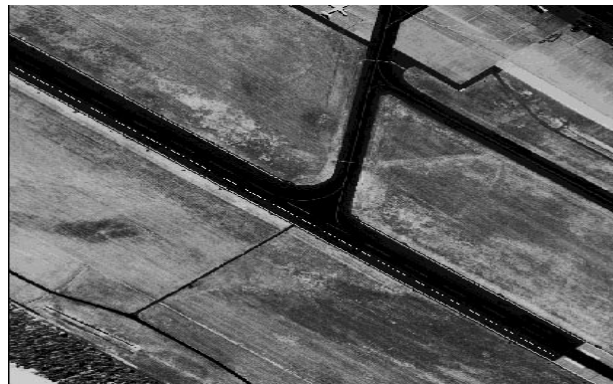


Figure 15: From this image, a line on the runway of the airport Nuremberg (crossing the picture from top left to bottom right) was cut out, the line is indicated by the dotted (or dashed) white line. The sun zenith angle is 32.4° . The flight direction is from bottom to top, so the scan direction is from left to right. A vertical line in the center of the picture corresponds to nadir ($\theta_r = 0^\circ$). Scan angles to the left are indicated by negative zenith angles in the plots above and correspond to $\varphi = 90.5^\circ$, scan angles to the right have positive zenith angles and correspond to $\varphi = 89.5^\circ$. The data are plotted for a wavelength band 630 to 690 nm.

Surface	a_0 [%]	a_1 [%·rad ⁻²]	a_2 [%·rad ⁻¹]
Runway	8.69	1.31	0.28
Highway	6.68	9.13	7.27

Table 2: Coefficients of the fits of model Walthall (angles are in radians) at a wavelength of 630 to 690 nm.

Figures 14 and 15 (both surfaces are made of asphalt) show the original and the corrected data with the respective fit of the Walthall model (equation 6) for channel 4, corresponding to a wavelength of 630 to 690 nm. Table 2 contains the coefficients of the respective fits. The remaining channels show the same characteristics as channel 4, the shape of the function is dominated by the coefficient a_1 .

Figure 14 shows the principal plane and very strong BRDF effects, a strong rise in backscatter as well as in specular direction. For the maximum scan angles, the reflectance is almost twice as high as for nadir reflectance. Unfortunately, the sun zenith angle $\theta_i = 59.2^\circ$ is much larger than the maximum scan angle ($\theta_r = 42.5^\circ$). The strongest effects in the principal plane are expected when $\theta_r = \theta_i$.

Figure 15 shows the cross principal plane and only small BRDF effects, a slight increase of about 10 % at high zenith angles. From the about 20 sample lines we investigated, most of them showed an increase for high zenith angles. The Walthall model is not well suited for our studies because of the limited angular distribution of the azimuth angle of the pixels on the lines, we are planning to use other empirical models to describe the angular dependencies of the reflectances in our Daedalus images too.

6 outlook

Further studies concerning the bidirectional behavior of man made surfaces are in progress. The BRDF of asphalt was measured under natural illumination. The bidirectional characteristics of urban areas shall be determined on multispectral image data from the Daedalus scanner. In August 1997 we obtained more Daedalus image data. This time the flight paths were chosen to meet the requirements of BRDF investigations. In these image data the same scene will be viewed from several (up to 5) angles for two different sun positions, so that much more different combinations of angles are available for fitting models.

Our long term goal is to develop a physical model to describe the BRDF's of man made surfaces. This will lead to a good estimate of the error made in processing images of urban areas with different view angles and improve classification algorithms. The surface topography of several materials will be measured with a height resolution of 0.16 μm for a detailed model of surface scattering.

REFERENCES

- [Bartsch, 1994] B. Bartsch and S. Bakan and J. Fischer, 1994. Remote Sensing of Water Vapour within the Solar Spectrum, SPIE (The International Society for Optical Engineering), 2311, pp. 197-206.
- [Hepp-94] T. Hepp, 1994. Erzeugung multispektraler Reflektanzbilder zur automatisierten Bildauswertung, diploma thesis, CENSIS Report 10-94, University of Hamburg, FRG.
- [Kollewe-96] T. Kollewe, 1996. Vergleich multispektraler Flugzeugscanneraufnahmen mit Reflektanzmessungen am Boden, diploma thesis, CENSIS Report 17-96, University of Hamburg, FRG.
- [Liang, 1994] S. Liang and A. H. Strahler, 1994. Retrieval of Surface BRDF from Multiangle Remotely Sensed Data, Remote Sensing of Environment, 50, pp. 18-30.
- [Meister, 1996] G. Meister, 1996. Messung der spektralen Reflexionsfunktion (BRDF) ausgewählter Oberflächen bei natürlicher Beleuchtung, diploma thesis, Universität Hamburg, II. Institut für Experimentalphysik, CENSIS-REPORT-18-96.
- [Nicodemus, 1970] F.E. Nicodemus, 1970. Reflectance Nomenclature and Directional Reflectance and Emissivity, Applied Optics, 9 (6), pp. 1474-1475.
- [Richter, 1994] R. Richter, 1994. Model SENSAT-5 Sensor-Atmosphere-Target, DLR-IB 552-01/94, DLR- Institute for Optoelectonics, Wessling/Munich, FRG.
- [Rothkirch, 1997] A. Rothkirch, 1997. Feldmessung der spektralen Reflexionsfunktion (BRDF) eines Hausdaches, diploma thesis, Universität Hamburg, II. Institut für Experimentalphysik, CENSIS-REPORT-30-96.
- [Walthall, 1985] C. L. Walthall and J. M. Norman and J. M. Welles and G. Campbell and B. L. Blad, 1985. Simple equation to approximate the bidirectional reflectance from vegetation canopies and bare soil surfaces, Applied Optics, 24, pp. 383-387.